Acta Geotechnica (2014) 9:181–186
DOI 10.1007/s11440-013-0233-8

RESEARCH PAPER

Thermomechanical effects of a rapid depressurization in a gas cavern

Pierre Bérest · Benoit Brouard · Hippolyte Djakeun-Djizanne · Grégoire Hévin

Received: 3 January 2013 / Accepted: 20 February 2013 / Published online: 26 September 2013

Abstract Rapid gas depressurization leads to gas cooling followed by slow gas warming when the cavern is kept idle. Gas temperature drop depends upon withdrawal rate and cavern size. Thermal tensile stresses, resulting from gas cooling, may generate fractures at the wall and roof of a salt cavern. However, in most cases, the depth of penetration of these fractures is small. These fractures are perpendicular to the cavern wall. The distance between two parallel fractures becomes larger when fractures penetrate deeper in the rock mass, as some fractures do not keep growing. These conclusions can be supported by numerical computations based on fracture mechanics. Salt slabs are created. However, these slabs remain strongly bounded to the rock mass and it is believed that in many cases their weight is not large enough to allow them to break off the cavern wall. Depth of penetration of the fractures must be computed to prove that they cannot be a concern from the point of view of cavern tightness.

Keywords Cavern thermodynamics · Gas caverns · Thermal stresses

1 Introduction

Gas storage caverns were developed mainly for seasonal storage, with one or a few cycles per year and a moderate gas production rate between the maximum and minimum operation pressure. However, the needs of energy traders are prompting change toward more aggressive operating modes. Typically, high-deliverability caverns can be emptied in 10 days and refilled in 30 days or less. Maximum pressure drop rates are expected to become faster. At the same time, compressed air energy storage (CAES) is experiencing a rise in interest. CAES facilities are designed to deliver full-power capacity in a very short time period. Both types of facilities (CAES and high-frequency cycled gas storage cavern, HFCGSC) imply high gas production rates and multiple yearly pressure cycles. This cycled mode of operation of solution-mined caverns raises questions regarding frequently repeated, extreme, mechanical and thermal loading.

P. Bérest (✉) · H. Djakeun-Djizanne
LMS, Ecole Polytechnique, Palaiseau, France
e-mail: berest@lms.polytechnique.fr

B. Brouard
Brouard Consulting, Paris, France

G. Hévin
Storengy, Bois-Colombes, France

2 Temperature changes in a gas cavern

2.1 Convection in a gas-filled cavern

In a gas cavern, pressure is almost uniform, as gas density is small (50–200 kg/m^3). Temperature distribution is a slightly more complicated problem. In a salt formation, rock thermal conductivity is $K_R = 5$–6 W/m/°C and the geothermal gradient typically is $G = 1.5$–1.8 °C/100 m. However, as gas (or liquid) conductivity is smaller than rock conductivity, the geothermal gradient at rest should be larger in the cavern fluid than in the rock mass.

In fact, it can be expected that gas effectively is stirred by thermal convection: temperature is warmer at the cavern bottom, gas is lighter, and gas is driven upward by gravity forces. However, natural convection only occurs when the geothermal gradient is larger than a certain threshold, the *adiabatic* gradient (G_{ad}). Considering the simple example

of a dry gas, $G_{ad} = g/C_P$ where $g = 10$ m/s^2 is the gravity acceleration, and C_P is the specific heat of gas (when pressure is kept constant). For natural gas, $C_P = 2{,}345$ J/kg/°C and for air, $C_P = 1{,}000$ J/kg/°C. In other words, $G > G_{ad}$ and, in principle, convection must appear in any cavern. However, G is not much larger than G_{ad}, and convection can be impeded in some cases—for instance, when warm gas is injected at the cavern top, when cold brine is left at the cavern bottom at the end of the leaching period, or when gas is cooled to a temperature colder than the temperature of the brine left at the cavern bottom. Examples can be found in Quast [22], Fosse and Røvang [13], Krieter et al. [17], Kneer et al. [16], Klafki et al. [15] and Skaug et al. [26]. When thermal convection develops, it is extremely effective. Dimensional analysis shows that convection is governed by the Prandtl number ($\mathrm{Pr} = \nu/k$, ν = kinematic viscosity, k = gas thermal diffusivity) and the Grashof number ($\mathrm{Gr} = g\alpha G a^4/\nu^2$), where a is the cavern characteristic length, and α is the thermal expansion coefficient. The Grashof number is quite high in a large cavern, and turbulent convection develops. In a *brine*-filled cavern, $G_{ad} = \alpha T g/C_P = 0.035$ °C/100 m: onset of convection is certain.

2.2 Heat balance equation

When it is assumed that gas absolute temperature, T, and pressure, P, are almost uniform throughout the entire cavern, the heat balance equation can be written (ATG [1]; this equation is at the base of the SCTS software developed for SMRI.):

$$m\left(C_P\dot{T} + \frac{1}{\rho^2}T\frac{\partial\rho}{\partial T}\bigg|_P\dot{P}\right) = \int_{\partial\Omega} -K_R\frac{\partial T_R}{\partial n}\mathrm{d}a + L\dot{C} + <\dot{m}> C_P\left(T_{inj} - T\right) \quad (1)$$

where ρ, m, T, P are gas density, mass, absolute temperature, and pressure, respectively; T_R is rock temperature. The gas-state equation can be written $P = \rho r T Z(P, T)$, where $Z = Z(P, T)$ is the gas compressibility factor. Kinetic energy is neglected. The left-hand side reflects the changes in internal energy minus the work of the external forces. The right-hand side is the sum of the heat flux crossing the cavern walls (discussed later; the evolution of temperature in the rock mass is governed by thermal conduction, $K_R = 5$–6 W/m/°C is the thermal conductivity of salt) plus the heat generated during condensation and vaporization of water vapor (this term is neglected in this paper; C is the mass of water vapor.) plus the enthalpy flux that enters the cavern during gas injection (T_{inj} is the temperature of the injected gas.) This flux vanishes when no gas is injected in the cavern, $\dot{m} < 0$ (withdrawal) or $\dot{m} = 0$ (standstill).

2.3 Gas withdrawal

In the following, simplifying assumptions are made. The boundary condition at cavern wall raises a difficult problem: it is likely that gas temperature gradient is large in a thin boundary layer at cavern wall whose thickness depends on wall roughness and on the rate of the convective gas flow. For simplicity, it is assumed that rock temperature at cavern wall equals gas temperature and that cavern walls are smooth (for a discussion of the effects of irregularities, see Krieter [18]). Only gas withdrawal is considered, $\dot{m} < 0$. The gas compressibility factor is $Z = 1$, and the gas-state equation writes $P = \rho r T$. Cavern compressibility is quite small when compared to gas compressibility and the cavern volume is assumed to remain constant. The case of an idealized spherical cavern, radius a, is considered. Equation (1) then can be re-written:

$$m(t)C_v\dot{T}(t) - \dot{m}(t)rT(t) = -4\pi a K_R\int_0^t \dot{T}(\tau)\left[1 + \sqrt{\frac{t_c}{(t-\tau)}}\right]\mathrm{d}\tau$$
$$T(t=0) = T_0 \quad (2)$$

$t_c = a^2/\pi k_R$ is the rock thermal diffusivity ($k_R = 3 \times 10^{-6}$ m^2/s is typical.), and $r = C_p - C_v$ is the difference between the specific heats of the gas at constant pressure and constant volume, respectively. In an actual cavern, the right-hand side of (2), or the heat flux crossing the cavern walls, cannot be neglected and the "adiabatic" solution, or $T/T_0 = (m/m_0)^{\gamma-1}$, where $\gamma = C_p/C_v$, does not apply. Dimensional analysis proves that, following withdrawal of a certain amount of gas (in % of the total gas inventory), gas temperature at the end of the withdrawal is lower when the withdrawal rate is faster or when the cavern is bigger.

2.4 Example

Crossley [11] describes a withdrawal test performed in a Melville (Canada) cavern. The measured flow rate, cavern pressure and temperature are drawn in Fig. 1. Equation (2) was used to compute pressure and temperature evolutions. The following values were selected: $\gamma = 1.27$ and $C_P = 2{,}347$ J/kg/°C. The cavern volume is $V = 46{,}153$ m^3, but its shape was unknown and the surface/volume area was (artificially) increased by a factor of 2 to reach a good fit between measured and computed values. Note that slightly before the end of the withdrawal phase (day 5), gas temperature starts warming, as heat flux from the rock mass becomes quite fast.

2.5 Depth of penetration of temperature changes

Solving Eqs. (1) or (2) allows computing temperature evolution. Generally speaking, penetration of temperature

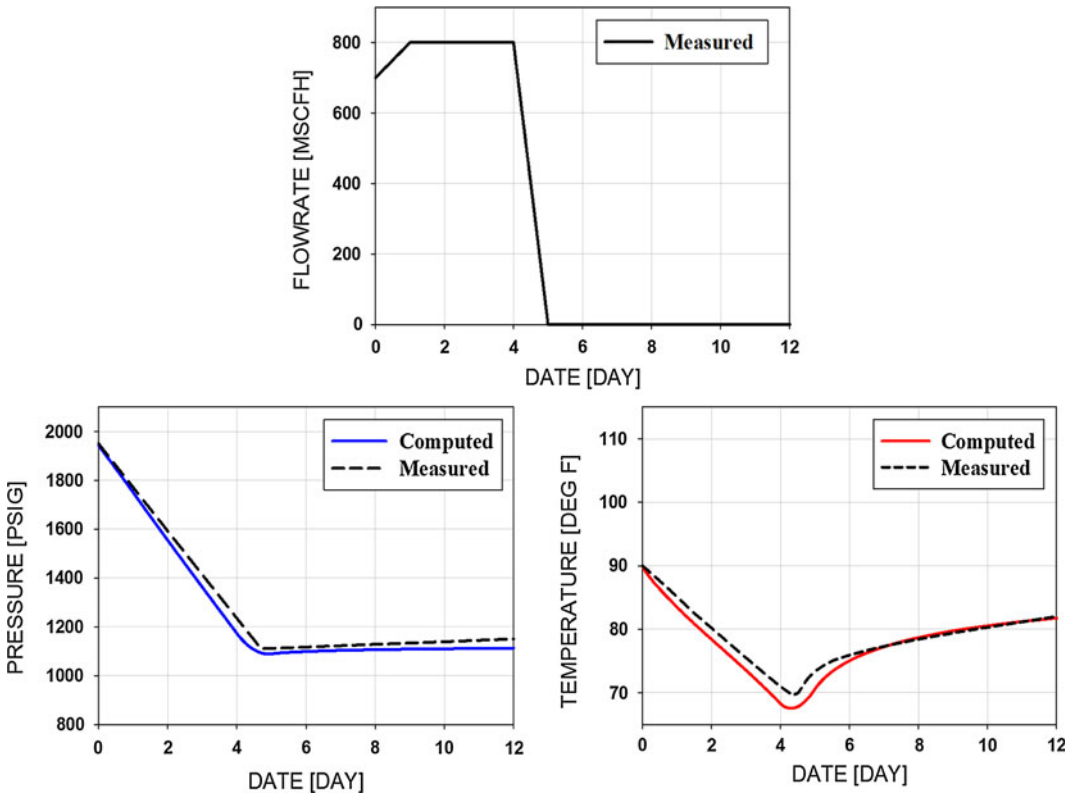

Fig. 1 Melville Cavern. Gas withdrawal rate, pressure and temperature evolutions, as observed and as computed by LMS (after Crossley [11])

changes in the rock mass is slow. For instance, when a cold gas temperature has been kept constant at the cavern wall during a t-long period of time, the rock temperature is changed significantly in a domain at a cavern wall with a thickness of $d = (k_R t)^{1/2}$, or $d \approx 3$ m after $t = 1$ month. Brouard et al. [8] considered a spherical cavern and applied a periodic temperature distribution at the cavern wall. They proved that accurate temperature computation requires that a refined mesh be used in the vicinity of the cavern wall. The temperature distribution as a function of the distance from the cavern wall when the gas temperature is minimal is shown in Fig. 2. Three cycling periods were considered: 1 day (CAES); 1 week; and 1 month (corresponding to an "aggressively" operated HFCGSC). In this last case, temperature fluctuations are divided by a factor of 10 at a 3-m distance from the cavern. (This distance is not strongly influenced by cavern radius.)

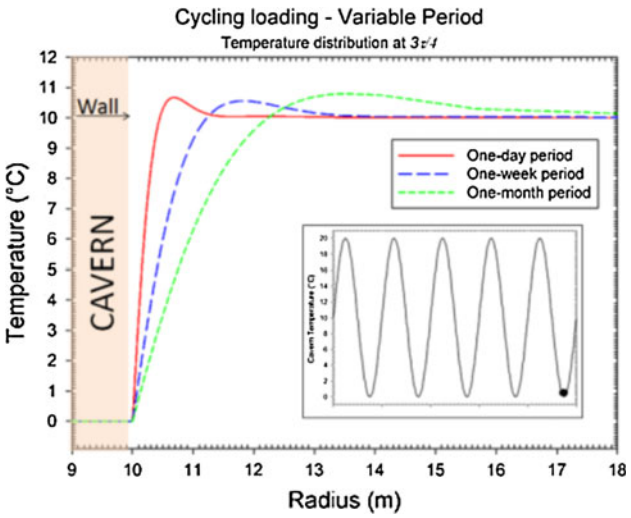

Fig. 2 Temperature distribution in the rock mass after 5 cycles, when gas temperature is lowest. Cavern temperature is periodic, varying from 0 to 20 °C. Three periods are considered: 1 day, 1 week and 1 month. After 5 cycles, a periodic temperature evolution is reached in the rock mass

3 Stress changes at cavern wall

3.1 "Thermal" stresses

Cooling (or warming) at the cavern wall generates thermal stresses. Orders of magnitudes can be computed easily. Let $\Delta T < 0$ be the difference between the rock temperature at the cavern wall and the virgin temperature (geothermal temperature) at cavern depth. Normal stresses generated by this difference are small (at the cavern wall, the thermal normal stress is zero.); however, tangential thermal stresses are of the order of $\sigma_{tt} = -E\alpha_R \Delta T/(1 - \nu)$, where

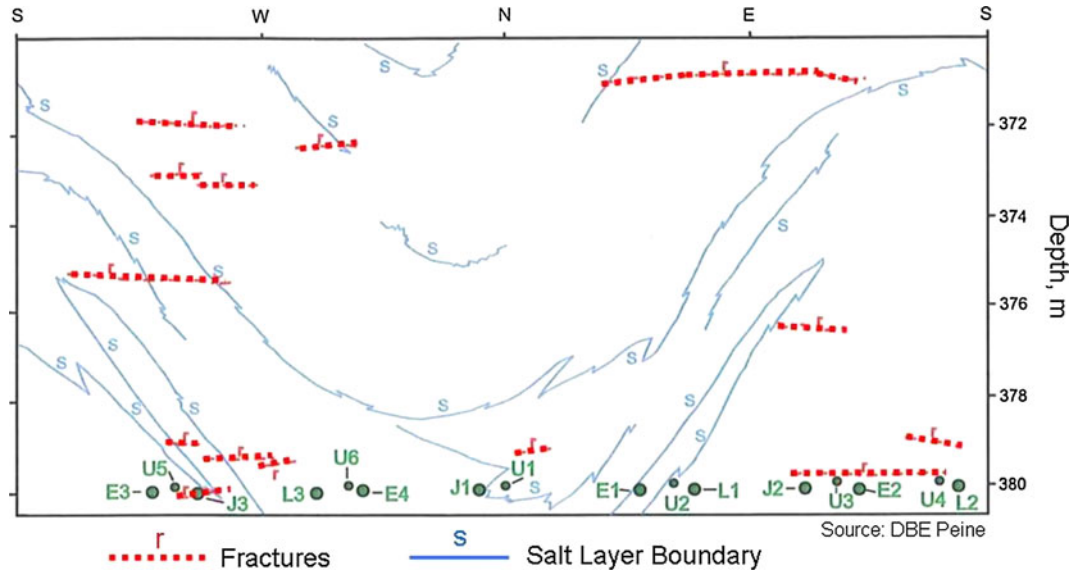

Fig. 3 Gorleben Mine. Thermal fractures at the wall of a ventilation shaft. Fractures are *horizontal* and fractures average spacing is 2.8 m. From Zapf et al. [28]

$E = 18{,}000$ MPa is the elastic modulus, $v = 0.25$ is the Poisson's ratio, and $\alpha_R = 4 \times 10^{-5}$/°C is the thermal expansion coefficient of the rock. When $\Delta T < 0$ (gas cooling), the tangential thermal stresses are tensile, and $-\sigma_t/\Delta T = 1$ MPa/°C. This is a very high figure, tensile stresses are so large that rock tensile strength of salt (1–2 MPa) is exceeded and fractures open.

3.2 Example: thermal fractures in a ventilation shaft

Wallner and Eickemeier [27] discussed the onset of fractures in an intake air shaft in a salt formation (Fig. 3). "During the cold season, temperatures in the shaft decreased by 20 °C … within a time period of 80 days… horizontal and vertical fractures were detected by routine inspections in the shaft. Theses fractures had an average spacing of about 2.8 m. The fracture aperture amounted up to several mm." (p. 365). This example was also discussed by Zapf et al. [28]. Rough computations explain such a phenomenon. The shaft is a cylinder, radius a. Let P_∞ be the geostatic pressure at shaft depth. It is assumed that steady-state mechanical behavior of the rock mass can be described by a power law

$$\dot{\varepsilon} = A\sigma^n,\ n = 3 \text{ to } 6$$

Steady-state creep closure is reached, and air temperature is cooled down by ΔT. At cavern wall, stresses can write [5]:

$$\sigma_{rr}(a) = 0, \sigma_{\theta\theta}(a) = -2P_\infty/n - E\alpha_R\Delta T/(1-v),$$
$$\sigma_{zz}(a) = -P_\infty/n - E\alpha_R\Delta T/(1-v) \quad (3)$$

This very simple model predicts that horizontal fractures appear first when $\Delta T < -(1-v)P_\infty/nE\alpha_R$. At a 600-m depth, $P_\infty = 13.2$ MPa, and when $n = 3$, he condition writes $\Delta T < -4.4$ °C.

3.3 Spalling in gas caverns

Is thermal fracturing a significant phenomenon in actual gas caverns? Several caverns experienced spalling, sluffing, break-outs and fast creep closure. Examples were discussed in the literature, see for instance Röhr [23], Baar [2], Serata and Cundey [25], Boucly and Legreneur [6], Coates et al. [9], Quast [22], Bérest et al. [4], Crotogino et al. [12], Hévin et al. [14], Rokahr et al. [24]. In most cases, these caverns were deep gas storage caverns in which gas pressure was low when the gas inventory was small. In a gas cavern, cavern shape evolution, cavern bottom rise and brine–gas interface rise can be measured, at least from time to time. However, interpretation of these measurements often is not unequivocal; for instance, both spalling *and* creep closure can contribute to cavern bottom rise. In several cases, break-outs were observed even when pressure change rates were relatively slow; in one case overhanging blocks fell down during the first gas injection; this may be attributed to the reduction in Archimedes thrust, when fluid density drastically drops after brine withdrawal; no or small further block fall was observed.

However, Cole [10] described the case of two gas caverns of the Markham storage field in Texas in which severe spalling was observed. These caverns were cycled 8–10 times per year. Withdrawal rates were 3–4 times faster than injection rates. Cavern tops are at 3,450 ft (1,050 m) and 3,531 ft (1,075 m), and the original cavern heights were 1,739 ft (530 m) and 2,284 ft (696 m), respectively. The

first gas injections were in June 1992 (Cavern #2) and October 1995 (Cavern #5). Cavern operation resulted in cavern volume loss and salt sluffing from the walls and roof of the cavern. Brine–gas interface surveys were run every year. As of January 2002, the caverns had lost 292 ft (89 m) and 419 ft (128 m) of their depths. A "material balance" test (the amount of withdrawn gas, pressure and temperature are carefully measured during such a test) also had been performed in 2001 to assess the cavern "free" volume, and natural gas sonar surveys were run in January 2002. Comparison of these various methods suggests that the cavern creep closure was approximately 5 % of the initial volume; however, a similar volume of salt had fallen from the walls to the bottom of the cavern. Comparison of sonar profiles proved that "no large sections of salt from one area of the caverns fell to the bottom creating the fill… the salt was removed in thin layers over large areas of the caverns… horizontal cavern closure occurred… thus closing in part of the area created by the salt falling.", Cole [10], p. 82. Such features are not fully consistent with the expected effects of thermal fracturing. Munson et al. [19] also described salt sluffing in oil storage caverns where no thermal effects can be expected. In other words, clear lessons are difficult to draw from case histories [5].

3.4 Fracture mechanics

In principle, Fracture Mechanics allow to predict the aperture, depth and spacing of thermal fractures [3, 20]. However, this domain is still a matter of researches. A few simple rules can be stated:

- Fractures are perpendicular to the cavern wall. In a cylindrical well, fractures are mostly horizontal.
- Fracture depth approximately equals the depth of the zone in which tensile stresses are larger than rock tensile strength (assuming that this strength is zero is on the safe side). Obviously, the development of fractures modifies the state of stress in the vicinity of the fractures; the tensile stresses addressed here are those stresses computed with the assumption that no fracture exists.
- At the beginning of the cooling process, when the depth of penetration of temperature changes is shallow, stresses are tensile in a thin zone at cavern wall and many thermal micro-fractures appear at cavern wall. When low temperatures penetrate deeper into the rock mass, the propagation of many fractures stops and only a small number of them continue to develop. This process is illustrated in Fig. 4.
- The ratio between fractures depth and fractures spacing is not very different from 1.

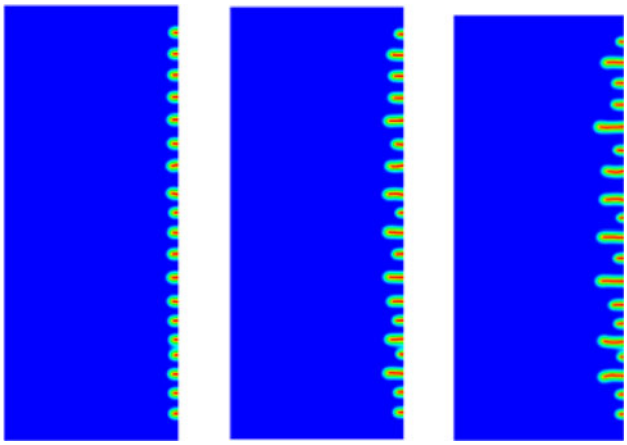

Fig. 4 Onset of fractures at a cylindrical cavern wall. A −5 °C temperature drop is applied at the cavern wall and kept constant. After some time, fractures appear at the cavern wall. As the cold temperature front penetrates deeper into the rock mass, a smaller number of fractures keep growing. (Computations by P. SicSic and J. J. Marigo, LMS, Ecole Polytechnique)

- The ratio between the aperture of a fracture, or o, and the spacing between two consecutive fractures, or s, typically is $o/s = -\alpha_R\ \Delta T$($\Delta T < 0$ is the temperature change at the cavern wall). In the case of the Gorleben shaft described above, $\Delta T = -20$ °C, $\alpha_R = 4 \times 10^{-5}$/°C, $s = 2.8$ m and fracture aperture can be expected to be $o = 2$ mm or so.

3.5 Effective tensile stresses

It was assumed that fractures can appear when a tangential tensile stress develops at the cavern wall. (The effect of gas pressure was not taken into account.) However, this criterion may be too optimistic. When performing a hydraulic fracturing test in a borehole, fluid pressure in the borehole is increased to a figure slightly higher than the geostatic pressure to create a fracture. Such tests are performed routinely to assess in situ stresses. When interpreting such tests, one must take into account the onset of *effective* tensile stresses. Effective stress is the sum of the actual compressive stresses (negative) plus the fluid pressure. When the least-effective stress is tensile (positive), the onset of fracturing is possible. This criterion is more severe than the no-tensile-stress criterion considered above. Whether such a criterion ("no effective tensile stress") must be taken into account is still open to discussion [7].

4 Conclusions

The thickness of the zone in which stresses are tensile can be computed through standard numerical computations.

Generally speaking, this zone is not very thick because gas never remains much colder than the rock mass during a very long period of time. An example was provided in Fig. 2. There is no significant risk of block fall, as the blocks delimited by two consecutive fractures remain strongly bounded to the rock mass [21]. However, some specific zones (such as non-convex parts of the cavern profile, or flat roofs whose span is large) are more prone to develop tensile stresses and can be subject to spalling, leading to a smoother profile of the cavern. They are not a real concern. Cavern tightness also must be considered. The distance between cavern top and salt roof must be significantly larger than the thickness of the possible tensile zone. Simple numerical computations allow checking that this criterion is met.

Acknowledgments This study was funded partially by the French *Agence Nationale de la Recherche* (ANR) in the framework of the SACRE Project, which includes researchers from EDF, GEOSTOCK, PROMES (Perpignan), HEI (Lille) and Ecole Polytechnique (Palaiseau).

References

1. ATG (1986) Stockages souterrains de gaz (Underground gas storages). Manuel pour le transport et la distribution du gaz, Titre XIII. Association technique de l'industrie du gaz en France, 62 rue de Courcelles, 75008 Paris France (In French)
2. Baar CA (1977) Applied salt-rock mechanics. Vol. I. Developments in geotechnical engineering. Elsevier Science, Amsterdam
3. Bahr HA, Weiss HJ, Bahr U, Hoffmann M, Fischer G, Lamperscherf S, Balke H (2010) Scaling behavior of thermal shock crack patterns and tunneling cracks driven by cooling or drying. J. Mech. Ph. Solids 58(2010):1411–1421
4. Bérest P, Ghoreychi M, Fauveau M, Lebitoux P (1986) Mechanism of creep in gas storage caverns. Effect of gravity forces. In: Hartman HL (ed) Proceedings of the 27th US symposium on Rock Mech. Soc. Min. Eng. Inc., Littleton, Colorado, pp 789–794
5. Bérest P, Djizanne H, Brouard B, Hévin G (2012) Rapid depressurizations: can they lead to irreversible damage?. SMRI Fall Meeting, Regina, pp 64–83
6. Boucly Ph., Legreneur J. (1980) Hydrocarbon storage in cavities leached out of salt formations. In: Proceedings of the international symposium subsurface space. Stockholm, Sweden, pp 251-257
7. Brouard B, Karimi-Jafari M, Bérest P (2007) Onset of tensile effective stresses in gas storage caverns. SMRI Fall Meeting, Halifax, pp 119–135
8. Brouard B, Frangi A, Bérest P (2011) Mechanical stability of a cavern submitted to high-frequency cycles. SMRI Spring Meeting, Galveston, pp 99–116
9. Coates GK, Lee CA, McLain WC, Senseny PE (1983) Closure and collapse of man-made cavities in salt. In: Proceedings of the 6th international symposium salt, pp 139–157
10. Cole R (2002) The long term effects of high pressure natural gas storage on salt caverns. SMRI Spring Meeting, Banff, pp 75–97
11. Crossley NG (1996) Salt cavern integrity evaluation using downhole probes. A transgas perspective. SMRI Fall Meeting, Cleveland, pp 21–54
12. Crotogino F, Mohmeyer KU, Scharf R (2001) Huntorf CAES: more than 20 years of successful operation. SMRI Spring Meeting, Orlando, pp 351–362
13. Fosse AP, Røvang LB (1998) Verifying established initial gas temperature distribution in caverns. SMRI Spring Meeting, New Orleans, pp 126–142
14. Hévin G, Caligaris C, Durup JG (2007) Deep salt cavern abandonment: a pilot experiment. SMRI Fall Meeting, Halifax, pp 16–25
15. Klafki M, Wagler T, Grosswig S, Kneer A (2003) Long-term downhole fibre optic temperature measurements and CFD modeling for investigation of different gas operating modes. SMRI Fall Meeting, Chester, pp 180–189
16. Kneer A, Irmer A, Riegel H, Klafki M (2002) Application of a CFD-Code for modeling of 3-D processes in salt caverns during gas withdrawal. SMRI Fall Meeting, Bad Ischl, pp 197–209
17. Krieter M, Hagoort J, Barnewold D (1998) Thermodynamic simulation of gas caverns for optimized production management. SMRI Fall Meeting, Roma, pp 309–325
18. Krieter M (2011) Influence of gas cavern's surface area on thermodynamic behaviour and operation. SMRI Fall Meeting, York, pp 179–184
19. Munson DE, Ehgartner B, Bauer S, Rautman C, Myers R (2004) Analysis of a salt fall in Big Hill Cavern 103, and a preliminary concept of salt dome structure. SMRI Spring Meeting, Wichita, pp 57–72
20. Nemat-Nasser S, Keer LM, PanharK S (1978) Unstable growth of thermally induced interacting cracks in brittle solids. Int J Solids Struct 14:409–430
21. Pellizzaro C, Bergeret G, Leadbetter A, Charnavel Y (2011) Thermomechanical behavior of stublach gas storage caverns. SMRI Fall Meeting, York, pp 161–178
22. Quast P (1983) L'installation de Huntorf: plus de trois années de fonctionnement de cavernes à air comprimé. Annales des Mines 190(5–6), 93–102 (In French)
23. Röhr HU (1974) Mechanical behavior of a gas storage cavern in evaporitic rocks. In: Coogan AH (ed) Proceedings of the 4th symposium on salt. Salt Institute, II, pp 93–100
24. Rokahr R, Staudtmeister K, Zander-Schiebenhöfer D, Johansen JI (2007) In-situ test with a gas storage cavern as a basis for optimization. SMRI Spring Meeting, Basel, pp 84–97
25. Serata S, Cundey TE (1979) Design variables in solution cavities for storage of solids, liquids and gases. In: Proceedings of the 5th symposium on salt. The Northern Ohio Geological Society Inc. Pub., pp 161–170
26. Skaug N, Ratigan J, Thompson M (2010) Natural gas cavern inventory assessment—a new approach. SMRI Spring Meeting, Gd Junction, pp 303–312
27. Wallner M, Eickemeier R (2001) Subsidence and fractures caused by thermo-mechanical effects. SMRI Spring Meeting, Orlando, pp 363–371
28. Zapf D, Staudtmeister K, Rokahr RB (2012) Analysis of thermal induced fractures in salt. SMRI Spring Meeting, Regina, pp 47–62